

Difference between Endocardial and Epicardial Application of Pulsed Fields for Targeting Epicardial Ganglia: An In-Silico Modelling Study

Francisco Estevez-Laborí¹, Barry O'Brien², Ana González-Suárez^{3,4}

¹ *Universidad Internacional de Valencia, Valencia, Spain*

² *AtriAN Medical Ltd., Galway, Ireland*

³ *Translational Medical Device Lab, School of Medicine, University of Galway, Ireland*

⁴ *iBIO, Escuela Superior de Ingeniería, Ciencia y Tecnología, Universidad Internacional de Valencia, Valencia, Spain*

Corresponding author: Dr. Ana González-Suárez, Translational Medical Device Lab, 2nd Floor, Lambe Translational Research Facility, University College Hospital Galway, Ireland. Email: ana.gonzalezsuarez@universityofgalway.ie

Funding details: This publication has emanated from research conducted with the financial support of Science Foundation Ireland under Grant number [22/PATH-S/10719] and the Spanish Ministerio de Ciencia e Innovación, Agencia Estatal de Investigación, Fondo Europeo de Desarrollo Regional (Grant PID2022-136273OA-C33 funded by MCIN / AEI / 10.13039/501100011033 / FEDER, UE) and the Universidad Internacional de Valencia-VIU under research project number (PII2024_115).

Conflicts of interest: Barry O'Brien is employee of AtriAN Medical, Galway, Ireland. The rest of the authors declare no conflict of interest.

Running title: Endocardial vs. epicardial pulsed field ablation

Data availability: Supplementary material (Excel file) includes the output data of the simulations, along with all the graphics created with this data that appear in the manuscript.

Abstract

Background: Pulsed Field Ablation (PFA) has recently been proposed as a non-thermal energy to treat atrial fibrillation by selective ablation of ganglionated plexi (GP) embedded in epicardial fat. While some of PFA-technologies use an endocardial approach, others use epicardial access with promising pre-clinical results. However, as each technology uses a different and sometimes proprietary pulse application protocol, the comparison between endocardial vs. epicardial approach is almost impossible in experimental terms. For this reason, our study, based on a computational model, allows a direct comparison of electric field distribution and thermal-side effects of both approaches under equal conditions in terms of electrode design, pulse protocol and anatomical characteristics of the tissues involved.

Methods: 2D computational models with axial symmetry were built for endocardial and epicardial approaches. Atrial (1.5–2.5 mm) and fat (1–5 mm) thicknesses were varied to simulate a representative sample of what happens during PFA ablation for different applied voltage values (1000, 1500 and 2000 V) and number of pulses (30 and 50).

Results: The epicardial approach was superior for capturing greater volumes of fat when the applied voltage was increased: 231 mm³/kV with the epicardial approach vs. 182 mm³/kV with the endocardial approach. In relation to collateral damage to the myocardium, the epicardial approach considerably spares the myocardium, unlike what happens with the endocardial approach. Although the epicardial approach caused much more thermal damage in the fat, there is not a significant difference between the approaches in terms of size of thermal damage in the myocardium.

Conclusions: Our results suggest that epicardial PFA ablation of GPs is more effective than an endocardial approach. The proximity and directionality of the electric field deposited using an epicardial approach are key to ensuring that higher electric field strengths and increased

temperatures are obtained within the epicardial fat, thus contributing to selective ablation of the GPs with minimal myocardial damage.

Keywords: Computer modelling; endocardial ablation; epicardial ablation; ganglionated plexi; pulsed field ablation

Introduction

Atrial Fibrillation (AF) is the most common cardiac arrhythmia, with most patients being highly symptomatic and at increased risk of stroke and heart failure [1]. Anti-arrhythmic drugs (AADs) offer only limited success and cause significant side-effects [2]. Catheter ablation has therefore become the preferred treatment approach in patients refractory to AADs or when the side-effects can no longer be tolerated. Ablation techniques have focused on electrically isolating the left atrium from the pulmonary veins, based on the observation that these veins were the main source of triggers that cause the arrhythmia [3]. Radiofrequency (RF) heating was initially the predominant technology for these pulmonary vein isolation (PVI) techniques, with low-temperature cryoballoon treatments being subsequently introduced. Both of these PVI technologies have provided very similar outcomes in terms of efficacy with modest 1-year success rates of approximately 65-70% in patients with paroxysmal AF [4] – outcomes in patients with persistent or permanent AF are usually lower [5].

Pulsed field ablation (PFA) technology [6] has recently been introduced and has already obtained regulatory approval in some jurisdictions. Several clinical trials have now been completed using a variety of different device designs [7-10]. One of the key benefits identified from these studies has been the improved safety profile of PFA compared to the traditional thermal methods; specifically the risk of the damage to the oesophagus [11] and the phrenic nerve [12] has been substantially reduced. From an efficacy perspective, results out to 1-year follow-ups are slightly better than the thermal approaches, with freedom from AF in the 66% [13] to 81% [14] range: though it is important to note that monitoring methodology during follow-up can notably influence recorded outcomes [15]. However, these efficacy outcomes are somewhat disappointing – higher success rates would have been expected considering the very high acute and medium term PV isolation rates observed in these studies.

The ablation success rates for conventional PVI have, at least in part, been attributed to collateral damage of epicardial ganglionated plexi (GP), reducing vagal inputs that can contribute to AF initiation and propagation [16]. This consideration is supported by evidence of abolition of the GP vagal response after PVI [17,18]. Interestingly, it has now been confirmed that the new PFA technologies do not abolish this vagal response, which is highly evident during energy delivery, but is still present after isolation is achieved [19,20]. This suggests that the pulsed electric field induced by PFA is strong enough to stimulate the GP, but is not sufficient to cause notable GP ablation, with the usual endocardial approach. On the other hand, there is pre-clinical evidence showing that pulsed electric fields can ablate GPs when the energy is delivered epicardially [21,22]. However the differences in pulse parameters between various treatments makes it difficult to infer that the method of approach (endocardial versus epicardial) alone could be a key factor to explain the observations around GP ablation. The objective of this current study was therefore to model the electric field distribution induced in the tissues for the two approaches, using identical pulse parameters, and to assess thermal side-effect in the tissues of interest i.e. the atrial cardiac tissue and the epicardial fat in which the GPs are embedded. So, this is the first computational study in which a direct quantitative comparison was conducted between endocardial and epicardial approach. Insights from this study should therefore help to further understand the benefit of an epicardial approach when targeting GPs and to appreciate if, going forward, endocardial PVI PFA combined with epicardial GP PFA would be needed to ensure better long-term outcomes.

Methods

The methodology was based on coupled electrical-thermal computational models to simulate endocardial and epicardial PFA of the target zone (epicardial fat). These are the first available computational models in which both approaches were compared to be able to understand pre-

clinical and clinical data about lack of effectiveness of targeting GPs from endocardial approach and suggest some directions about how the process could be optimised. The numerical method was being newly applied to quantify the thermal-side effects of PFA and the collateral thermal damage in the myocardium from both approaches. This is impossible to quantify and predict with pre-clinical and clinical studies.

Model geometries

Figure 1 shows the two-dimensional limited-domain computational models with axial symmetry built for endocardial and epicardial approaches, which considered only the region of interest around the ablation catheter. Since these models had rotational symmetry, they were simulating three-dimensional scenarios. In addition, the feasibility of the limited-domain model has been previously demonstrated in comparison with a full torso model [23]. Both endocardial and epicardial approaches used a conventional cardiac ablation catheter design (7 Fr –4 mm) placed over different layers. The electrode-tissue pressure was considered to be constant and producing an insertion depth of 0.25 mm (which would be equivalent to a low contact force [24]). For the endocardial approach, the catheter was within the cardiac chamber surrounded by circulating blood and placed over the myocardium, fat and connective tissue (see Fig. 1A). On the other hand, for the epicardial approach, the catheter was placed over saline, fat, myocardium and circulating blood (Fig. 1B). This saline layer between the catheter and the fat (target) acts as a ‘virtual electrode’ to ensure the transmission of electrical energy into the target tissue [21]. To adhere to the constraints of a 2D axisymmetric model, the electrode was considered to be perpendicular to the tissue surface throughout the treatment. To account for the anatomical variations encountered in the adult population, different thicknesses for the fat and the myocardium layers were considered [25]. In both approaches the fat layer was varied from 1 to 5 mm, since in a previous study it was noted that fat layers ≥ 1 mm were more

effective to reach the target [26], but the limit on this was not established. Myocardium thickness was varied within anatomical ranges from 1.5 to 2.5 mm [25].

A model verification analysis was conducted to determinate the optimal outer dimensions of blood and connective tissue. The value of the volume of tissue affected by PFA was considered as a control parameter. To determine these dimensions, we increased their values by equal amounts and when the difference in volume between consecutive simulations was less than 1%, we considered the former values to be adequate. We then determined the adequate spatial resolution by means of similar analysis using the same control parameter. Discretization was spatially heterogeneous, where the finest zone was the electrode-tissue interface since the largest voltage gradient was produced and hence the maximum value of current density. In the tissue, grid size increased gradually with distance from the electrode-tissue interface. This verification analysis provided a width of 80 mm and height of 40 mm of the outer dimensions of blood and connective tissue. The optimal meshing of the models had 3,444 and 2,150 triangular elements for endocardial and epicardial approach respectively, with a minimum element size of 0.006 mm at the electrode-tissue interface.

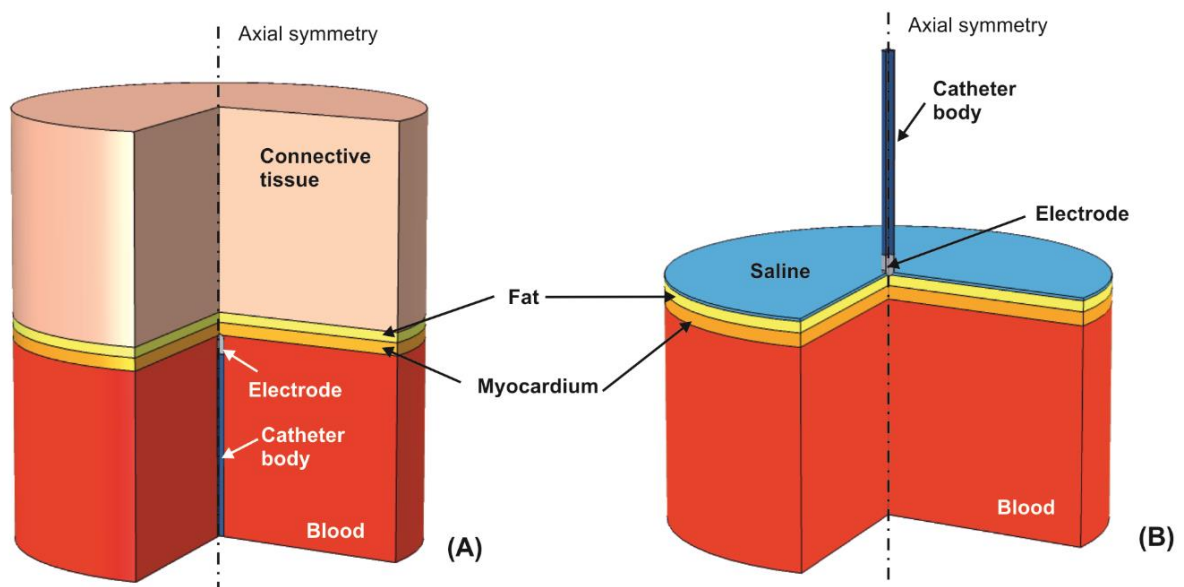


Figure 1. Geometries of the 2D limited-domain models with axial symmetry for endocardial **(A)** and epicardial **(B)** approach. The ablation catheter in both scenarios was embedded 0.25 mm into the myocardium and saline layer respectively.

Governing equations

The models were based on a coupled electrical-thermal problem, which were solved numerically by the Finite Element Method (FEM) with COMSOL Multiphysics (COMSOL, Burlington, MA, USA). A quasi-static approximation was employed for the electrical problem. The transient cellular responses were not considered (i.e. membrane charging), then the electric field distribution can be computed by solving Maxwell's equations in its Laplacian form [27]:

$$\nabla \cdot (\sigma \nabla \phi) = 0 \quad (1)$$

$$\mathbf{E} = -\nabla \phi \quad (2)$$

$$\mathbf{J} = \sigma \mathbf{E} \quad (3)$$

where σ is the electrical conductivity of the material, ϕ the electrical voltage, \mathbf{E} the electric field vector, and \mathbf{J} the current density vector.

The thermal problem was considered to evaluate any possible thermal side-effect during epicardial and endocardial PFA. This problem was solved by using the Bioheat Equation [28]:

$$\rho c \frac{\partial T}{\partial t} = \nabla \cdot (k \nabla T) + Q + Q_p + Q_{met} \quad (4)$$

where ρ is density (kg/m^3), c specific heat ($\text{J}/\text{kg}\cdot\text{K}$), T temperature ($^{\circ}\text{C}$), t time (s), k thermal conductivity ($\text{W}/\text{m}\cdot\text{K}$), Q the heat source caused by the electrical power associated with PFA (W/m^3), Q_p the heat loss caused by blood perfusion (W/m^3) and Q_m the metabolic heat generation (W/m^3). Both Q_m and Q_p were ignored as these terms are negligible compared to the others [28], especially for short duration heating [29].

Material properties

The electrical and thermal properties of the models' elements are shown in Table 1 [30-32]. The electrical conductivity of the connective tissue (all the tissue surrounding the heart) was estimated by considering a mixture of 50% of fat and 50% muscle, which represents a good approximation to what was observed in CT-scans of patients [31]. The electrical conductivity changes dynamically with the electric field as the cell becomes more permeable to electrical current when PFA-induced pores are created. Due to the increase of the number of applied pulses, the cumulative effect of temperature would also promote the increase of tissue conductivity. Therefore, the electrical conductivity was modelled as a function of both the local electric field and temperature [33-35], which was defined as follows:

$$\sigma(\mathbf{E}, T) = \sigma_0 \cdot \left[\left(1 + A \cdot \text{flc2hs}(\mathbf{E} - E_{del}, E_{range}) \right) + \alpha \cdot (T - T_0) \right] \quad (5)$$

where σ_0 the initial conductivity (pre-electroporation conductivity), A is the increase factor of the conductivity after the electroporation (the post-electroporation conductivity σ_1 is equal to $\sigma_0(1 + A)$), flc2hs is a smoothed Heaviside with a continuous second derivative implemented in COMSOL, E_{del} is the middle point of the transition zone, E_{range} the value of the transition zone, α ($1/^\circ\text{C}$) is the coefficient that reflects the conductivity change due to temperature variation, and T_0 is the initial temperature (37°C). Therefore, the function $\sigma(\mathbf{E})$ increases from σ_0 to σ_1 with the transition zone from $E_{del} - E_{range}$ (RE, reversible threshold) to $E_{del} + E_{range}$ (IRE, irreversible threshold). We considered a value of α of $+2\%/^\circ\text{C}$ as indicated in the literature [36]. The initial pre- and post-electroporation conductivities were considered to be equivalent to those measured at 10 Hz and 500 kHz (σ_0 and σ_1 , respectively) as was justified in [23]. The post-electroporation conductivity considered was within the β -dispersion frequency range (1 kHz-100 MHz) [37,38]. The IRE threshold for the simulations was 1000 V/cm as was recently reported for irreversible damage of the myocardium [39]. Due to the lack of available data for

RE threshold of the myocardium, we assumed a value of 500 V/cm as it is in concordance with the threshold obtained for other tissues such as liver with pulses of 100 μ s [40].

Table 1. Electrical and thermal properties of the model elements [30-32].

Element/Material	σ_0 (S/m)	σ_1 (S/m)	k (W/m·K)	ρ (kg/m ³)	c (J/kg·K)
Electrode/Pt-Ir	$4.6 \cdot 10^6$		71	21500	132
Catheter/Polyurethane	10^{-5}		23	1440	1050
Saline	1.392		0.628	980	4184
Epicardial fat/adipose tissue	0.0377	0.0438	0.21	911	2348
Heart/myocardium	0.0537	0.281	0.56	1081	3686
Cardiac chamber/Blood	0.7		0.52	1050	3617
Connective tissue*	0.1199		0.35	1000.5	2884.5

σ : Electrical conductivity (σ_0 and σ_1 being the pre- and post-electroporation electrical conductivity values, respectively); k : thermal conductivity; ρ : density; c : specific heat.

* Mixture of 50% fat and 50% muscle

Boundary conditions

Electrical and thermal boundary conditions were applied over the limits of the models. Regarding electrical boundary conditions, PFA settings consisted of applying a pulse train based on a sequence of 30 monophasic pulses of 100 μ s width and 1 Hz frequency using monopolar configuration, i.e., the energy was applied between the metal catheter tip and the dispersive electrode, as done in pre-clinical studies [21,22]. The amplitude of the monophasic

pulses was varied between 1000 to 2000 V. We also assessed the effect of increasing the number of pulses to 50. To model these configurations, an electrical boundary condition to simulate the pulse train was applied at the metal tip catheter, while 0 V was set at the dispersive electrode. The dispersive electrode was defined in all the outer surfaces for the endocardial approach as well as in the epicardial approach except on the upper surface of the saline layer which was electrically isolated (i.e. electrical current was set to zero in this surface).

For thermal boundary conditions, a thermal convection coefficient of $1417 \text{ W/m}^2\cdot\text{K}$ ($37 \text{ }^\circ\text{C}$ temperature) at the myocardium-blood interface and at the electrode-blood interface (in the case of epicardial approach) was applied to simulate blood circulation, which was calculated under conditions of high blood velocity of 24.4 cm/s [41,42]. In the epicardial approach, two more thermal convection coefficients were applied: $20 \text{ W/m}^2\cdot\text{K}$ ($21 \text{ }^\circ\text{C}$ room temperature) at the air-electrode and air-saline interfaces to simulate air free circulation [30]; and $85 \text{ W/m}^2\cdot\text{K}$ ($37 \text{ }^\circ\text{C}$ body temperature) at the fat-saline interface for considering saline circulation through catheter ports at 2 mL/min [22]. For both approaches, the outer surfaces of the models were thermally isolated.

Analysed outcomes

Simulations were conducted to assess the electric field and temperature distributions of PFA using both approaches (endocardial and epicardial). In order to determine the PFA-induced electric effects, we assessed the volume of the fat (target) subjected to values of electric field above 1000 V/cm [39], which provided a metric of PFA-induced lesion size. Likewise, we evaluate any possible collateral electric field damage in the myocardium by quantifying the volume of myocardium subjected to values of electric field above 1000 V/cm . As for thermal effects, we assessed if there was any thermal-side effect provoked by PFA. To do that, the maximum temperature evolution in the fat and myocardium as well as temperature distributions

for both approaches were registered for all the voltage levels and number of pulses. The contour of the thermal lesion was assessed by means of the Arrhenius Equation, which establishes a relationship between the rate of thermal damage accumulation and the temperature, defining the degree of tissue damage:

$$\Omega(T, t) = A \int_0^t e^{-\frac{\Delta E}{R \cdot T(\tau)}} d\tau \quad (6)$$

where A is the frequency factor ($7.39 \times 10^{39} \text{ s}^{-1}$) and ΔE is the activation energy ($2.557 \times 10^5 \text{ J/mol}$) [43]. We considered $\Omega = 1$ as the thermal lesion contour, which represents 63% of dead cells.

Statistics

This study used a physics-based mechanistic model, where we assumed an uncertainty in the thicknesses of the atrial wall (1.5–2.5 mm) and the fat epicardial layer (1–5 mm) to simulate a representative sample of what happens during PFA ablation, under endocardial and epicardial approaches, and different applied voltage values (1000, 1500 and 2000 V). The normality of the data was checked using Shapiro-Wilk Test. The comparison of outcomes between both approaches was performed using the paired t-test for normally distributed data. In case of non-normal distribution, the comparison was carried out using the Wilcoxon Signed-Rank-test. The relationship between the outcomes and the applied voltage values was studied by simple regression using Excel. Coefficient of determination (R^2) was reported to assess the goodness of fit. Statistical significance was assumed when the P-value (P) was lower than 0.05.

Results

Electric field distribution for endocardial and epicardial approaches

Figure 2 shows the volume of fat captured within a 1000 V/cm isoline, using the endocardial and epicardial approaches, for the different voltages. The volume was the same for both 30 and 50 pulses, as shown in the Supplementary Material. It was observed that a significantly larger volume of electric field ($P < 0.05$) was created in the fat using the epicardial approach, for each voltage level, suggesting that this is more effective than the endocardial technique for capturing ablation targets within the fat. In this respect, as shown in Figure 3, the captured volume within the fat showed a direct linear correlation with the voltage applied, being strong for endocardial approach ($R^2 = 0.76$) and moderate for epicardial approach ($R^2 = 0.59$). In both cases this correlation was statistically significant ($P < 0.001$).

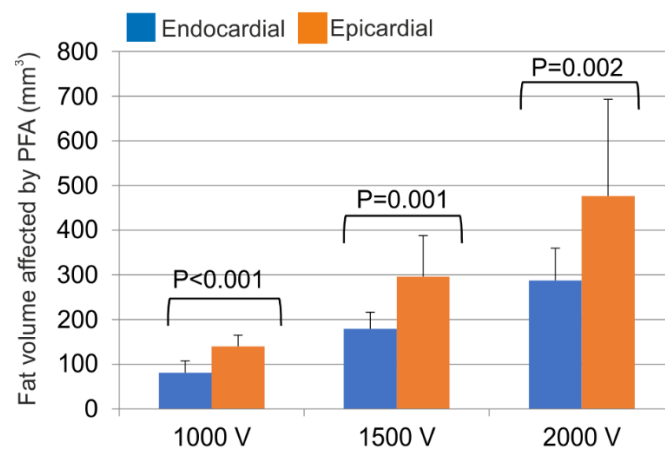


Figure 2. Volume of fat retained within a 1000 V/cm isoline for endocardial and epicardial approaches at different applied voltages.

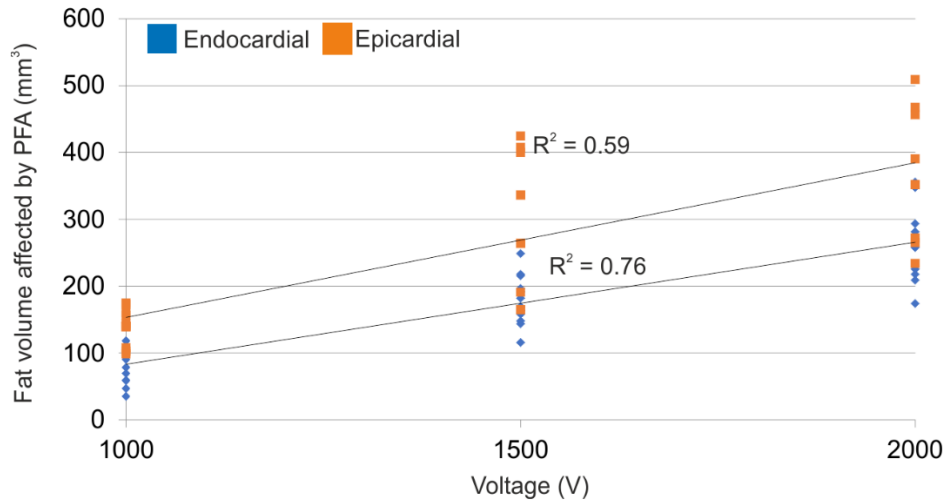


Figure 3. Relationship between the volume of fat captured by a 1000 V/cm isoline and the applied voltage for endocardial ($R^2=0.76$) and epicardial ($R^2=0.59$) approaches.

We also quantified the volume of the myocardium within the 1000 V/cm isoline using both approaches. As shown in Figure 4, the captured volume in the myocardium was significantly greater for the endocardial approach, regardless of the voltage level applied. This myocardial volume showed a strong linear correlation with the applied voltage for the endocardial approach ($R^2=0.96$), whereas the opposite was true for the epicardial approach ($R^2=0.28$), as shown in Figure 5.

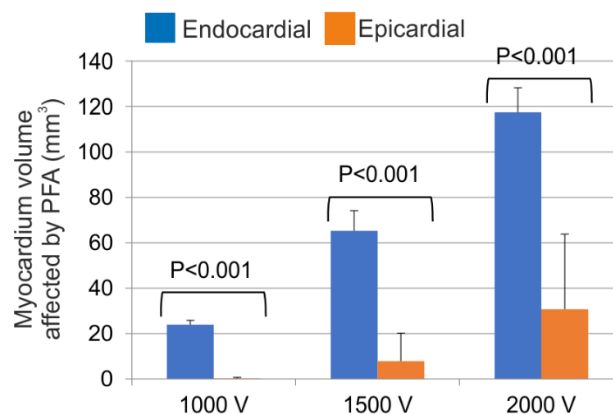


Figure 4. Volume of myocardium retained with a 1000 V/cm isoline for endocardial and epicardial approaches at different applied voltages .

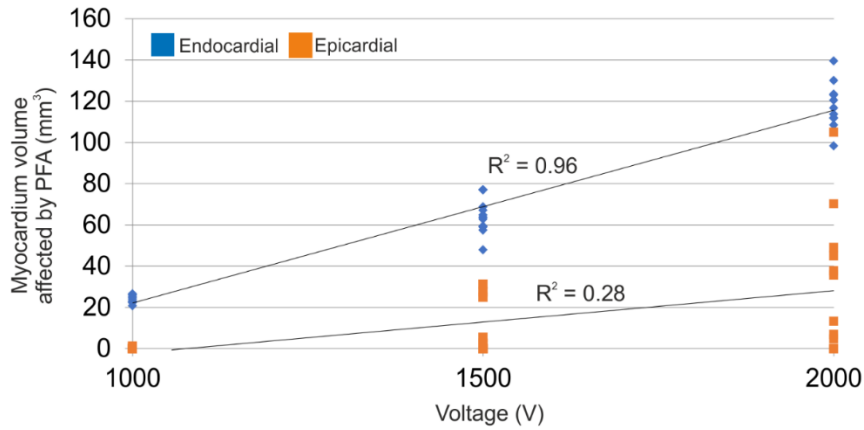


Figure 5. Relationship between the volume of myocardium captured by a 1000 V/cm isoline and the applied voltage for endocardial and epicardial approaches.

Temperature distribution for endocardial and epicardial approaches

Figure 6 shows the maximum temperature evolution in the epicardial fat and the myocardium for both epicardial and endocardial approaches, at the different applied voltages, for up to 50 pulses. In this instance, the fat and myocardium layer thickness was 1.5 mm and 2 mm, respectively. It was observed that the maximum temperature increased with higher voltages and with an increased number of pulses, for both fat and myocardium with both endocardial and epicardial approach. This increment as a function of time (i.e. as the number of pulses increased) was more pronounced within the first 10 pulses, particularly for the epicardial approach, then tended to stabilize after 30–40 s.

Regarding the endocardial approach (Fig 6A,C,E), the maximum temperature in the myocardium (green line) reached higher values than in the fat (blue line), especially at the beginning of the PFA treatment. The heating curve in the myocardium showed very sharp temperature spikes, relating to the pulse delivery. This effect was more marked for higher applied voltages and the greater number of pulses applied, with spike values of up to 65 °C developing in the myocardium at 2000 V. However, the final temperature in the fat typically remained below than 50 °C, even at 2000 V.

Unlike the endocardial approach, the temperature spikes reached in the fat during epicardial energy delivery were significantly higher than in the myocardium (Fig 6B,D,F). This phenomenon was more significant at higher applied potentials. When 50 pulses at 1500 V were applied, the temperature in the fat reached levels suggesting cell death ($> 50\text{ }^{\circ}\text{C}$), but the myocardial temperature remained within safe thermal levels. However, when the applied pulse is raised to 2000 V, both the myocardium and the fat reach temperatures that exceeded $50\text{ }^{\circ}\text{C}$.

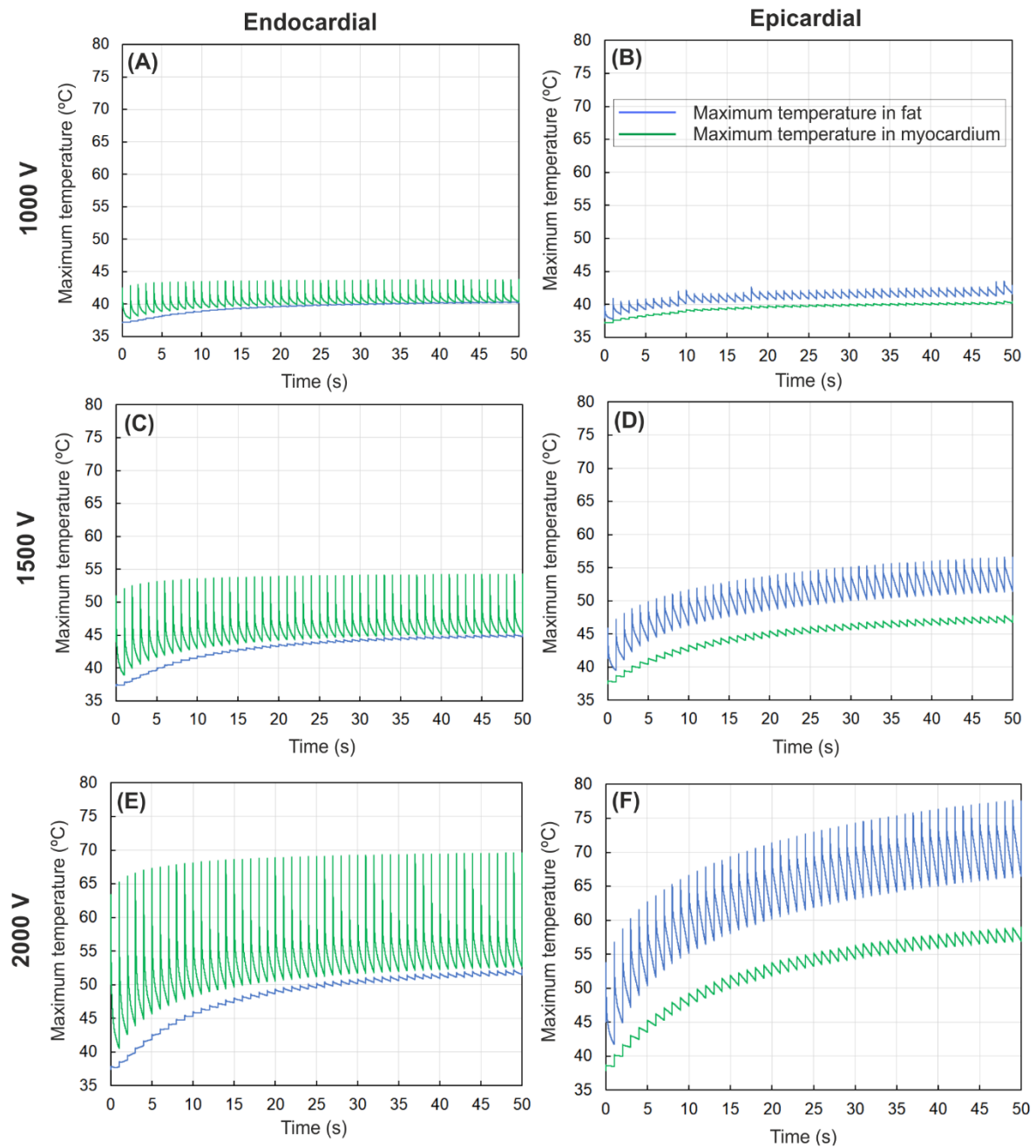


Figure 6. Evolution of the maximum temperature in the fat (blue colour) and myocardium (green colour) for both epicardial and endocardial approaches, for a fat layer of 1.5 mm and myocardium thickness of 2 mm, for different applied voltages (1000, 1500 and 2000 V) and up to 50 pulses.

Figure 7 shows the temperature distribution and thermal damage for both epicardial and endocardial approaches, increasing the voltage from 1000 to 2000 V and the number of pulses applied from 30 to 50. Again, this is for a scenario of 1.5 mm fat and 2 mm myocardium thickness. It is observed that when 1000 V is applied (Fig. 7A,B), the heating zone was below 45 °C and was located mainly in the surroundings of the electrode tip, regardless of the employed approach. There is no evidence of thermal damage irrespective of the number of pulses applied.

By increasing the applied voltage to 1500 V (Fig. 7C,D), the heating zone was extended further from the electrode tip reaching temperatures around 55 °C. This heating was more extensive in the fat layer for the epicardial approach. Thermal damage was observed in the fat when 50 pulses were applied – but only for the epicardial energy delivery.

As the voltage is increased to 2000 V (Fig. 7E,F), there is significant thermal damage in both approaches. Nevertheless, this thermal damage occurred at different sites depending on the energy delivery approach: while the myocardium was damaged during the endocardial approach, the fat (and minimally the myocardium) was damaged during the epicardial approach. The thermal lesion was greater in the epicardial case, since there was less power ‘lost’ via the blood pool. The number of pulses also affected the spread of the thermal damage; the damage extending mostly further into the fat in the epicardial case and mostly further through the myocardium in the endocardial case, when 50 pulses were applied.

Figure 8 shows the volume of tissues thermally damaged by PFA using the endocardial and epicardial approaches, at different applied voltages and pulses. (It is noted that there is no thermal damage in any case at 1000 V, regardless of the number of pulses.) At 1500 V, thermal damage was observed in the fat for the epicardial approach, even for only 30 pulses, albeit within a small volume. Thermal damage in the myocardium occurred only at 2000 V, without significant differences between both approaches ($P>0.05$). Using 30 pulses at 2000 V there was no notable thermal damage in the fat using an endocardial approach. While some thermal damage to the fat occurred with 50 pulses for the endocardial approach, there was a great difference in the extent of the damage compared to the epicardial approach.

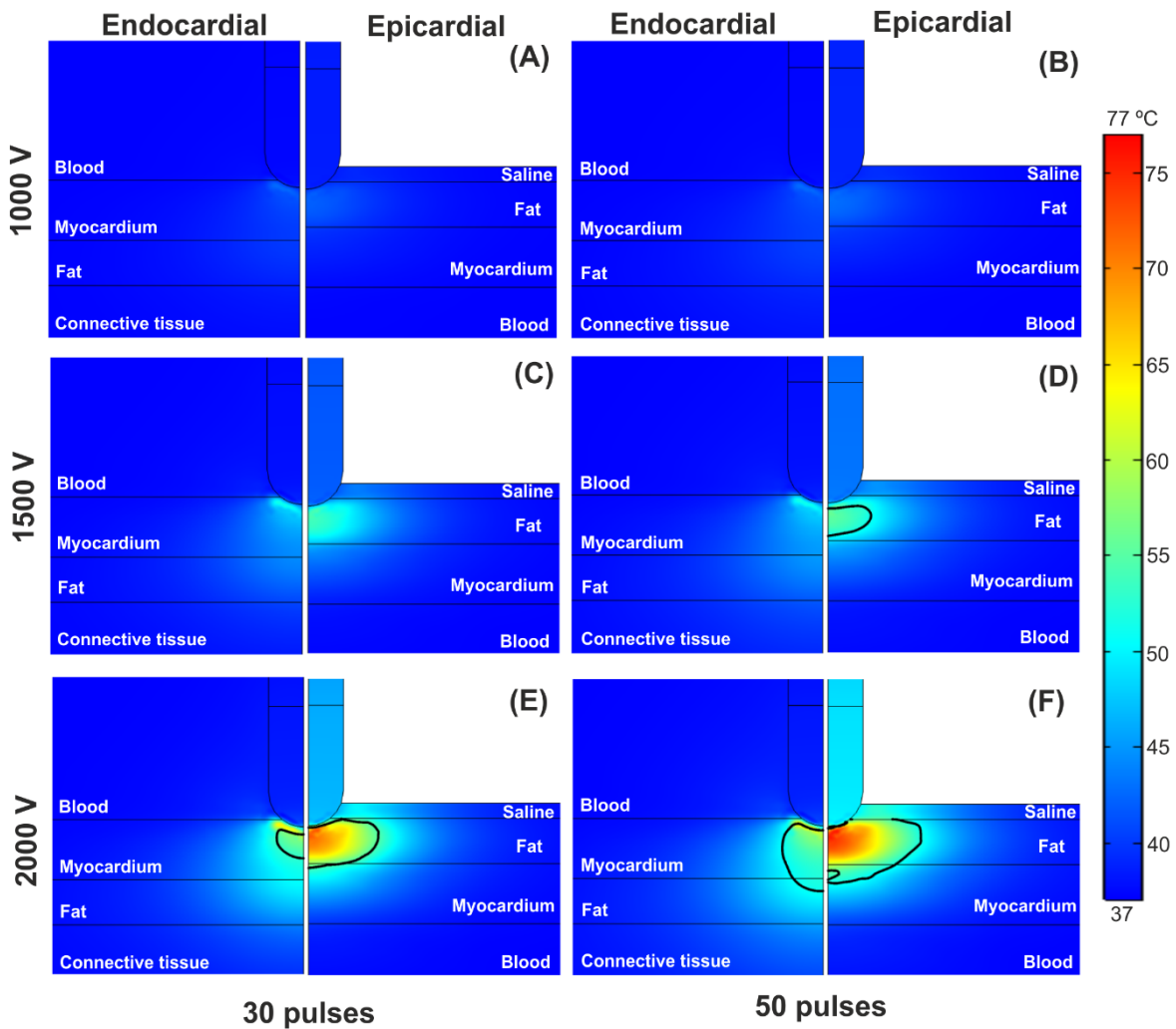


Figure 7. Temperature distribution for epicardial and endocardial approach for the case of 1.5 mm fat and 2 mm myocardium using different applied voltages (1000, 1500 and 2000 V) and number of pulses (30 and 50). The solid black line represents the thermal damage contour $\Omega = 1$.

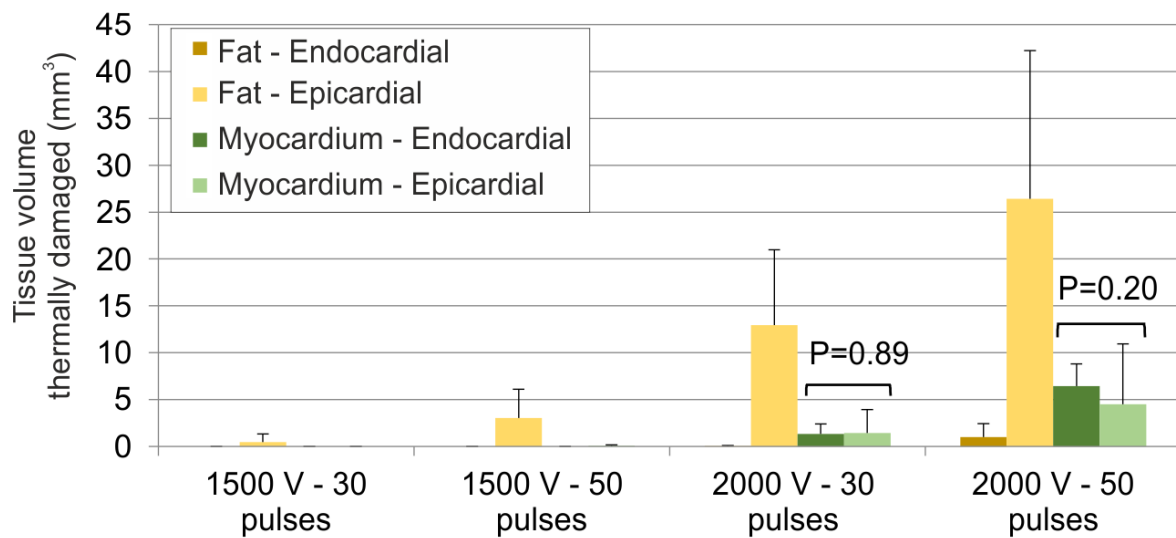


Figure 8. Volume of tissues thermally damaged by PFA in endocardial and epicardial approaches for different voltage applied (1000, 1500 and 2000 V) and number of pulses (30 and 50).

Effect of fat thickness for endocardial and epicardial approaches

Figure 9 shows the volume of electric field within the fat and myocardium captured within a 1000 V/cm isoline, using endocardial and epicardial approaches, when fat thickness was increased from 1 to 5 mm. It is observed that the volume of fat affected by PFA was greater as the thickness of fat increased, regardless of the approach used. Although this volume showed stronger correlation with thickness in for the epicardial approach (R^2 of 0.99 vs 0.70 for endocardial and epicardial approaches respectively).

On the other hand, the captured volume of myocardium was reduced with increasing fat thickness for both approaches. Although the myocardium volume showed a moderate

correlation with the fat thickness for the epicardial approach ($R^2 = 0.65$), there was practically no correlation for the endocardial approach.

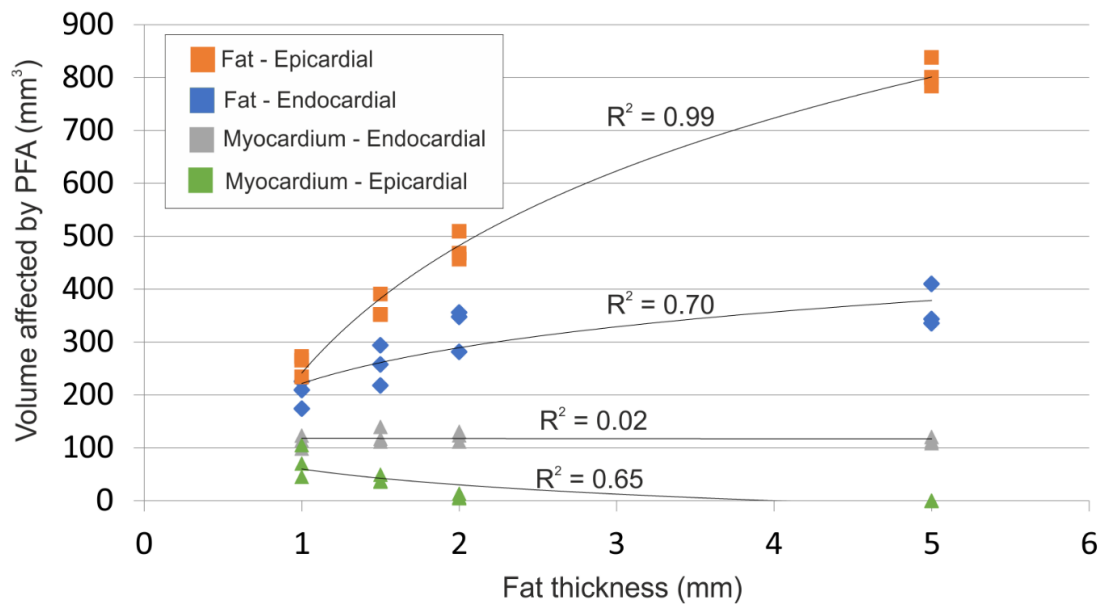


Figure 9. Volume of fat and myocardium retained within a 1000 V/cm isoline for endocardial and epicardial approaches for different fat thicknesses.

Regarding thermal effects with increasing fat thickness, Figure 10 shows the temperature distribution and thermal damage for both epicardial and endocardial approaches in presence of a fat layer of 5 mm (using the same myocardium thickness as in Figure 7), when the voltage was increased from 1000 to 2000 V and the number of pulses applied from 30 to 50. It can be observed that the maximum temperature remained below 50 °C for voltages up to 1500 V, regardless of the approach considered. When the voltage is raised to 2000 V, only the endocardial approach shows notable change, with a maximum temperature in the myocardium of around 60 °C, with 30 pulses applied. However, based on the thermal damage contour, notable damage was only reached in the myocardium when 50 pulses were applied using an endocardial approach.

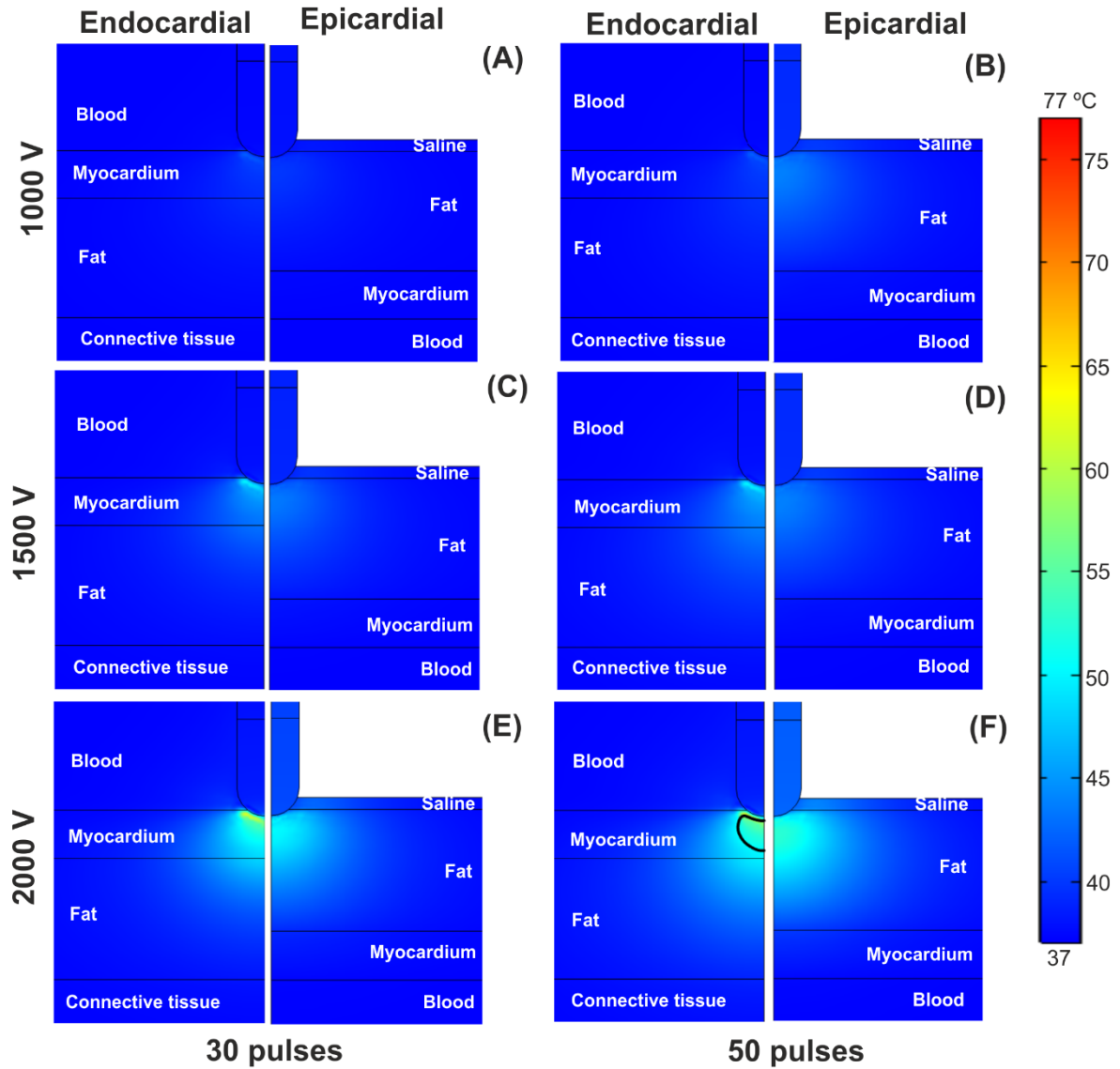


Figure 10. Temperature distribution for epicardial and endocardial approach for the case of 5 mm fat and 2 mm myocardium thickness using different applied voltages (1000, 1500 and 2000 V) and number of pulses (30 and 50). The solid black line represents the thermal damage contour $\Omega = 1$.

Discussion

Since the ganglionated plexi (GPs) are embedded in epicardial fat, it seems reasonable to assume a priori that an epicardial approach for GP ablation would be more effective than endocardial techniques i.e. more of the epicardial fat (and therefore the GPs) is likely to be exposed to higher electric fields than if the field is delivered from an endocardial location. For this reason, previous recent studies had focused on the epicardial approach to treat Atrial Fibrillation [44]. However, clinical and pre-clinical studies have also shown that the endocardial approach produced effective results [45, 46]. To be able to determine which approach would be the most appropriate for each particular case and treatment, other factors such as the thicknesses of the tissues involved (fat, myocardium, blood, connective tissue) or the possible thermal side-effects must also be taken into account. Computational modelling allows us to quantify these differences between the epicardial and endocardial approach.

Our results show a 65–73% larger PFA-affected fat volume in the epicardial case (see Fig. 2). Moreover, with both approaches, our results also suggest a moderate correlation between the PFA-affected fat volume and the applied voltage value: $R^2=0.76$ for endocardial and $R^2=0.59$ for epicardial (see Fig. 3). The greater the applied voltage, the greater the captured fat volume for both approaches. However, we observed a superiority of the epicardial approach for capturing greater volumes of fat when the applied voltage is increased: $231 \text{ mm}^3/\text{kV}$ with the epicardial approach vs. $182 \text{ mm}^3/\text{kV}$ with the endocardial approach.

Regarding how the myocardium could be collaterally damaged by PFA, our results suggest that the epicardial approach considerably spares the myocardium: there was hardly any myocardial tissue within the 1000 V/cm isoline at 1000 V , while at 1500 V and 2000 V the volume of myocardium captured was only 12% and 25% of the retained fat volume respectively (see Fig.

4). Conversely, the endocardial approach mainly damages the myocardium, perhaps not reaching the fat layer sufficiently, and therefore not successfully ablating the GPs.

Both the epicardial and endocardial approaches show a direct correlation between the volume of affected myocardium within the 1000 V/cm isoline and the applied voltage (see Fig. 5). However, within the fat volume, the correlation was very strong for the endocardial approach ($R^2=0.96$), but weak ($R^2=0.28$) for the epicardial approach (see Fig. 5). This difference seems logical given the close proximity and contact between the myocardium and the electrodes in the endocardial approach, which minimizes the disruption to the fat.

When considering increases in fat thickness, the epicardial approach is more effective than endocardial at capturing the increased volume of fat. This is also associated with a reduction in the volume of collateral myocardium captured when ablating epicardially. It is expected that capturing larger volumes of fat will be beneficial from the perspective of GP ablation; as these GP structures reside predominantly within the epicardial fat, increased fat capture will mostly likely improve efficacy of their ablation, giving improved clinical outcomes. Previous attempts at GP ablation used RF energy, delivered endocardially or epicardially. However, outcomes were confounded by damage to the myocardium around the GPs – this damage induced additional arrhythmia, mostly atrial tachycardia [47]. Thus, sparing the myocardium is important to ensure that the optimum benefit is obtained from the GP ablation. While GP ablation efficacy can only be inferred from the electric field data, it would indeed appear that the epicardial approach can well tolerate variations in epicardial fat from patient to patient.

In relation to the temperature changes induced by the pulsed field, our results show that high voltage pulses (> 1500 V) produce temperature spikes that are not negligible (see Fig. 6). It has been previously reported that PFA is not completely non-thermal therapy and that adjacent tissues could be affected by Joule heating, which is proportional to the square of the current

induced in the tissue and its application time [48]. Consequently, our results show that the oscillatory behaviour of the temperature spikes relates directly to the pulsed application of voltage. We also found that: 1) the peak values are greater in the myocardium for the endocardial approach, and are greater in the fat for the epicardial approach, and 2) the amplitude of the spikes is smaller for points deeper in the tissue, i.e. for fat in the endocardial approach, and for myocardium in the epicardial approach.

The temperatures reached for high voltages (> 1500 V) suggest the creation of a thermal lesion, which is supported by the results of the Arrhenius model (see Fig. 7). Here we observe that an increase in the number of pulses (from 30 to 50) results in larger volume lesions. Additionally, there is a tendency for the epicardial approach to create larger lesions, which is visually summarized in Fig. 8, where it is confirmed that the epicardial approach causes much more thermal damage in the fat than the endocardial approach. However, it also suggests that there is not a significant difference between the approaches in terms of size of thermal damage in the myocardium. Overall, the epicardial positioning of the catheter is indeed a key factor; this gives better proximity to the target ganglia (within the fat) and delivers the electric field directly into the fat. This is unlike endocardial delivery (out through the myocardium) where field losses occur at the myocardium-fat interface [48]. While PFA is generally more forgiving (than RF or cryo) in terms of contact with the tissue, delivery of the electric field into the fat is improved by a low level of saline irrigation at the electrodes; the epicardial model captures this, with the electrode making full contact with the saline. The endocardial model also describes full contact between the myocardium and the electrode.

The findings of this study may have important clinical implications suggesting, that when using PFA, an epicardial approach is more effective for ablating GPs compared to endocardial techniques. In the context of targeting just the GPs, the epicardial approach is also probably safer in terms of creating less collateral myocardial damage than the endocardial approach;

while not statistically significant (Figure 8) the trend can be seen in Figures 7 and 10. The models validates the findings of pre-clinical studies that have shown how epicardial PFA can selectively ablate the GPs with minimal myocardial damage [21, 22]; while inherent cellular electroporation thresholds of cardiomyocytes and neuron cell bodies may play a role in the selectivity [49], clearly the proximity and direction of the electric field delivery are also key elements. Additionally, the study helps to understand why endocardial PFA is not ablating even some of the ganglia, as had been the case for RF endocardial PVI. The long-term implications of not collaterally damaging the GPs during PVI are largely unknown, but it may lead to reduced treatment durability.

While endocardial RF ablation has been used to specifically target GPs for atrial fibrillation, with some successes [50], the approach carries a high risk of oesophageal damage. Endocardial RF is also being used to target GPs for syncope treatment [51], though given the improved safety that PFA provides it is difficult to see the continued use of RF for these patients.

The findings of the thermal models are also interesting when considering how the observed temperature changes may influence both cell death and electroporation thresholds. Even where a modest temperature increase in the fat were observed (at the lower voltages) it is possible that this increase leads to a local reduction in the electroporation threshold of the neuron cell bodies within the GPs. Thus the observation of selective GP ablation with epicardial PFA may also involve a contribution from localized temperature effects with the epicardial fat.

Limitations

Due to the limitations of using a 2D axisymmetric model, certain simplifications had to be made, leading to constraints on the scope and conclusions of the work. One issue lies in the assumption that the electrode maintains a perpendicular orientation to the tissue surface

throughout the treatment, a condition not always clinically relevant. This limitation arises from the dynamic nature of the beating heart during the procedure and the external manipulation of the catheter. The catheter's angle may change in response to these factors. Additionally, the study did not take into consideration variations in electrode-tissue pressure, which influence the depth of electrode penetration. Subsequent research endeavours will delve into a more comprehensive examination of these intricacies.

While this study used identical pulse parameters for both endocardial and epicardial field delivery (in order to isolate fundamental differences), the parameters used are not necessarily representative of real clinical devices and thus interpretation in relation to real-world clinical implications may be influenced by this. Different pulse trend characteristics might be necessary to achieve optimal results using the epicardial or endocardial approach. Perhaps, in the future, endocardial PVI PFA combined with epicardial GP PFA will be needed to ensure a better long-term outcome. Additionally, the study captured ranges in myocardial and fat tissue thicknesses, though further variations may be observed clinically. Ablation of GPs is inferred from the electric fields and temperatures determined – the models do not specifically capture GP ablation directly.

Finally, simulations were conducted using a monopolar configuration from both the epicardial and the endocardial approach. In a preliminary computational and preclinical work [52], we demonstrated that a bipolar configuration is feasible and effective to ablate GPs from an epicardial approach. Although with this mode the volume of fat reached was lower than with a monopolar application, there was less collateral volume of myocardium affected. It would be interesting as future scope to assess whether a bipolar configuration could enhance effectiveness of the endocardial approach to target GPs.

Conclusions

This modelling study has demonstrated how epicardial PFA ablation of GPs is more effective in capturing greater volumes of epicardial fat (where GPs are located) than endocardial ablation approaches, with 231 mm³/kV vs. 182 mm³/kV for epicardial and endocardial approach respectively. The proximity and directionality of electric field deposited using the epicardial approach are crucial for ensuring higher electric field strengths and increased temperatures within the epicardial fat, thereby contributing to the selective ablation of the GPs with minimal myocardial damage. The captured myocardium constituted only 12% and 25% of the retained fat volume at 1000 V and 1500-2000 V respectively.

References

1. J. Kornej, C.S. Borschel, E.J. Benjamin, R.B. Schnabel. Epidemiology of Atrial Fibrillation in the 21st Century – Novel Methods and New Insights. *Circulation Research* 2020; 127: 4-20.
2. P. Zimetbaum. Antiarrhythmic Drug Therapy for Atrial Fibrillation. *Circulation* 2012; 125: 381-389.
3. M. Haissaguerre, P. Jais, D. Shah, A. Takahashi, M. Hocini, G. Quiniou, S. Garrigue, A. Le Mouroux, P. Lr Metayer, J Clementy. Spontaneous initiation of atrial fibrillation by ectopic beats originating in the pulmonary veins. *N. Engl. J. Med.* 1998; 339: 659-666.
4. K.H. Kuck, J. Brugada, A. Furnkranz, A. Metzner, F. Ouyang, K.R.J. Chun, A. Elvan, T. Arentz, K. Bestehorn, S. Pockock et al. Cryoballoon or Radiofrequency Ablation for Paroxysmal Atrial Fibrillation. *N. Eng. J. Med.* 2016; 374, 2235-2245.
5. A. Verma, C. Jiang, T.R. Betts, J. Chen, I. Deisenhofer, R. Mantovan, L. Macle, C.A. Morillo, W. Haverkamp, R. Weerasooriya et al. Approaches to Catheter Ablation for Persistent Atrial Fibrillation. *N. Eng. J. Med.* 2015; 372: 1812-1822.
6. A. Sugrue, E. Maor, F. Del-Carpio Munoz, A.M. Killu, S.J. Asirvatham. Cardiac ablation with pulsed electric fields: principles ad biophysics. *Europace* 2022; 24: 1213-1222.
7. V.Y. Reddy, S.R. Dukkipati, P. Neuzil, A. Anic, J. Petru, M. Funasko, H. Cochet, K. Minami, T. Breskovic, I. Sikiric et al. Pulsed Field Ablation of Paroxysmal Atrial Fibrillation. 1-Year Outcomes of IMPULSE, PEFCAT, and PEFCAT II. *JACC Clin. Electrophysiol.* 2021; 7: 614-627.
8. V.Y. Reddy, P Peichl, E. Anter, G. Rackauskas, J. Petru, M. Funasako, K. Minami, J.S. Koruth, A. Natale, P. Jais et al. A Focal Ablatio.n Catheter Toggling Between Radiofrequency and Pulsed Field Energy to Treat Atrial Fibrillation. *JACC Clin. Electrophysiol.* 2023; doi: <https://doi.org/10.1016/j.jacep.2023.04.002>
9. M. Duytschaever, T. De Potter, M. Grimaldi, A. Anic, J. Vijgen, P. Neuzil, H Van Herendael, A Verma, A. Skanes, D. Scherr et al. Paroxysmal Atrial Fibrillation Ablation Using a Novel Variable-Loop Biphasic Pulsed Field Ablation Catheter Integrated With a 3-Dimensional Mapping System: 1-Year Outcomes of the Multicenter inspIRE Study. *Circ. Arrhythm. Electrophysiol.* 2023; doi: <https://doi.org/10.1161/CIRCEP.122.011780>
10. A. Verma, D.E. Haines, L.V. Boersma, N. Sood, A. Natale, F.E. Marchlinski, H. Calkins, P. Sanders, D.L. Packer, K-H. Kuck et al. Pulsed Field Ablation for the Treatment of Atrial Fibrillation: PULSED AF Pivotal Trial. *Circulation* 2023; 147(19): 1422-1432.
11. H. Cochet, Y. Nakatani, S. Sridi-Cheniti, G. Cheniti, F.D. Ramirez, T. Nakashima, C. Eggert, C. Schneider, R. Viswanathan, N. Derval et al. Pulsed field ablation selectively spares the oesophagus during pulmonary vein isolation for atrial fibrillation. *Europace* 2021; 23: 1391-1399.
12. F. Pansera, S. Bordignon, F. Bologna, S. Tohoku, S. Chen, L. Urbanek, B Schmidt, K.R.J. Chun. Catheter ablation induced phrenic nerve palsy by pulsed field ablation – completely impossible? A case series. *Eur Heart J Case Rep* 2022; <https://doi.org/10.1093/ehjcr/ytac361>
13. A. Verma, D.E. Haines, L.V. Boersma, N. Sood, A Natale, F.E. Marchlinski, H. Calkins, P. Sanders, D.L. Packer, K-H. Kuck et al. Pulsed Field Ablation for the Treatment of Atrial Fibrillation: PULSED AF Pivotal Trial. *Circulation* 2023; 147(19): 1422-1432.
14. M. Turagam, P. Neuzil, B. Schmidt, B. Reichlin, K. Neven, A. Metzner, J. Hansen, Y. Blaauw, P. Maury, T. Arentz et al. Safety and Effectiveness of Pulsed Field Ablation to Treat Atrial Fibrillation: One-Year Outcomes from the MANIFEST-PF Registry. *Circulation* 2023; 147: <https://doi.org/10.1161/CIRCULATIONAHA.123.064959>
15. M. Aguilar, L. Macle, M.W. Deyell, R. Yao, N.M. Hawkins, P. Khairy, J.G. Andrade. Influence of Monitoring Strategy on Assessment of Ablation Success and Postablation Atrial Fibrillation Burden Assessment: Implications for Practice and Clinical Trial Design. *Circulation* 2022; 145: 21-30.
16. K. Takahashi, I Watanabe, Y. Okumura, .K Nagashima, R Watanabe, M. Arai, K. Iso, S. Kurokawa, K. Okubo, T. Nakai et al. Effect of Cryoballoon Ablation vs. Radiofrequency Ablation on Left Atrial Ganglionated Plexi in Patients with Atrial Fibrillation. *J. Nihon Univ. Med. Ass.* 2018; 77(2): 87-91.
17. M. Qin, X. Liu, W-F. Jiang, S-H. Wu, X-D. Zhang, S. Po. Vagal response during pulmonary vein isolation: Re-recognized its characteristics and implications in lone paroxysmal atrial fibrillation. *Int. J. Cardiol.* 2016; 211: 7-13.
18. P. Garabelli, S Stavrakis, J.F.A. Kenney, S. Po. Effect of 28-mm Cryoballoon Ablation on Major Atrial Ganglionated Plexi. *J. Am. Coll. Cardiol.* 2018; 4: 831-838.
19. D. Musikantow, P. Neuzil, P. Petru, J. Koruth, S. Kralovec, M. Miller, M. Funasako, M. Chovanec, M. Turagam, W. Whang et al. Pulsed Field Ablation to Treat Atrial Fibrillation: Autonomic Nervous System Effects. *JACC Clin. Electrophysiol.* 2023; 9: 481-493.

20. P. Stojadinovic, D. Wichterle, P. Peichl, H. Nakagawa, R. Cihak, J Haskova, J Kautzner. Autonomic Changes Are More Durable after Radiofrequency than Pulsed Electric Field Pulmonary Vein Isolation. *J. Am. Coll. Cardiol.* 2022; 8: 895-904.
21. D. Padmanabhan, N. Naksuk, A. Killu, S. Kapa, C. Witt, A. Sugrue, C. DeSimone, M. Madhavan, J.R. de Groot, B. O'Brien et al. Electroporation of epicardial autonomic ganglia: Safety and efficacy in medium term canine models. *J. Cardiovasc. Electrophysiol.* 2019; 30: 607-615.
22. M. van Zyl, M. Khabsa, J. Tri, T. Ladas, O. Yasin, A. Ladejobi, J. Reilly, B.O'Brien, K. Coffey, A. Asirvatham. Open-Chest Pulsed Electric Field Ablation of Cardiac Ganglionated Plexi in Acute Canine Models. *J. Innov. Card. Rhythm. Manag.* 2022; 13(7): 5061-5069.
23. González-Suárez A, Irastorza RM, Deane S, O'Brien B, O'Halloran M, Elahi A. Full torso and limited-domain computer model for epicardial pulsed electric field ablation. *Comput Methods Programs Biomed* 2022 Jun;221:106886. doi: 10.1016/j.cmpb.2022.106886. Epub 2022 May 13.
24. Yan S, Gu K, Wu X, Wang W. Computer simulation study on the effect of electrode-tissue contact force on thermal lesion size in cardiac radiofrequency ablation. *Int J Hyperthermia.* 2020;37(1): 37-48. doi:10.1080/02656736.2019.1708482.
25. Sánchez-Quintana D, López-Mínguez JR, Macías Y, Cabrera JA, Saremi F. Left atrial anatomy relevant to catheter ablation. *Cardiol Res Pract.* 2014;2014:289720. doi: 10.1155/2014/289720. Epub 2014 Jun 24. Erratum in: *Cardiol Res Pract.* 2020 Aug 11;2020:3490543. PMID: 25057427; PMCID: PMC4095734.
26. González-Suárez A, O'Brien B, O'Halloran M, Elahi A. Pulsed electric field ablation of epicardial autonomic ganglia: computer analysis of monopolar electric field across the tissues involved. *Bioengineering* 2022;9(12):731.
27. Sheehan MC, Srimathveeravalli G. Pulsed electric fields. Principles and Technologies for Electromagnetic Based Therapies. In *Principles and Technologies for Electromagnetic Energy Based Therapies.* Prakash P, Srimathveeravalli G (Eds.). Elsevier Academic Press. 2021. ISBN: 9780128205945, pp: 71-106.
28. Berjano EJ. Theoretical modeling for radiofrequency ablation: state-of-the-art and challenges for the future. *Biomed Eng Online.* 2006 Apr 18;5:24. doi: 10.1186/1475-925X-5-24.
29. Pérez JJ, González-Suárez A, Berjano E. Numerical analysis of thermal impact of intramyocardial capillary blood flow during radiofrequency cardiac ablation. *Int J Hyperthermia.* 2018 May;34(3):243-249. doi: 10.1080/02656736.2017.1336258. Epub 2017 Jun 18. PMID: 28554240.
30. González-Suárez A, Pérez JJ, O'Brien B, Elahi A. In Silico Modelling to Assess the Electrical and Thermal Disturbance Provoked by a Metal Intracoronary Stent during Epicardial Pulsed Electric Field Ablation. *J Cardiovasc Dev Dis* 2022 Dec 14;9(12):458. doi: 10.3390/jcdd9120458.
31. Ramiro M Irastorza, Timothy Maher, Michael Barkagan, Rokas Liubasuskas, Juan J Pérez, Enrique Berjano, Andre d'Avila. Limitations of Baseline Impedance, Impedance Drop and Current for Radiofrequency Catheter Ablation Monitoring: Insights from In silico Modeling. *J Cardiovasc Dev Dis* 2022 Oct 3;9(10):336. doi: 10.3390/jcdd9100336.
32. Hasgall P.A., Di Gennaro F., Baumgartner C., Neufeld E., Lloyd B., Gosselin M.C., Payne D., Klingensböck A., Kuster N. It Is Database for Thermal and Electromagnetic Parameters of Biological Tissues, Version 4.1, 22 February 2022. [(accessed on 11 November 2022)]. Available online: <https://itis.swiss/virtual-population/tissue-properties/overview/>
33. Guo F, Deng H, Qian K, Li X. Characterization of dispersion and anisotropic-conductivity in tissue model during electroporation pulses. *Bioelectrochemistry.* 2022 Apr;144:108029. doi: 10.1016/j.bioelechem.2021.108029. Epub 2021 Dec 2.
34. Y. Zhao, S. Bhonsle, S. Dong, Y. Lv, H. Liu, A. Safaai-Jazi, R.V. Davalos, C. Yao, Characterization of Conductivity Changes During High-Frequency Irreversible Electroporation for Treatment Planning, *IEEE Trans. Biomed. Eng.* 65 (2018) 1810–1819, <https://doi.org/10.1109/TBME.2017.2778101>.
35. Y. Zhao, R.V. Davalos, Development of an endothermic electrode for electroporation-based therapies: A simulation study, 117 (2020) 143702. <https://doi.org/10.1063/5.0019743>.
36. Duck, F. A. (2013). *Physical Properties of Tissues: a Comprehensive Reference Book.* Cambridge, MA: Academic press.
37. Aycock KN, Zhao Y, Lorenzo MF, Davalos RV. A Theoretical Argument for Extended Interpulse Delays in Therapeutic High-Frequency Irreversible Electroporation Treatments. *IEEE Trans Biomed Eng.* 2021 Jun;68(6):1999-2010. doi:10.1109/TBME.2021.3049221. Epub 2021 May 21.
38. Neal RE et al., "In vivo characterization and numerical simulation of prostate properties for non-thermal irreversible electroporation ablation," *Prostate*, vol. 74, no. 5, pp. 458–468, 2014.
39. Avazzadeh, S.; O'Brien, B.; Coffey, K.; O'Halloran, M.; Keane, D.; Quinlan, L.R. Establishing irreversible electroporation electric field potential threshold in a suspension in vitro model for cardiac and neuronal cells. *J. Clin. Med.* 2021, 10, 5443.
40. Sel, D.; Cukjati, D.; Batiuskaite, D.; Slivnik, T.; Mir, L.M.; Miklavcic, D. Sequential finite element model of tissue electroporation. *IEEE Trans. Biomed. Eng.* 2005, 52, 816–827.

41. Tungjitkusolmun S, Vorperian VR, Bhavaraju N, Cao H, Tsai JZ, Webster JG. Guidelines for predicting lesion size at common endocardial locations during radio-frequency ablation. *IEEE Trans. Biomed. Eng.* 2001, 48, 194–201.
42. González-Suárez A, Berjano E. Comparative analysis of different methods of modeling the thermal effect of circulating blood flow during RF cardiac ablation. *IEEE Trans. Biomed. Eng.* 2016, 63, 250–259.
43. Irastorza RM, d'Avila A, Berjano E. Thermal latency adds to lesion depth after application of high-power short-duration radiofrequency energy: Results of a computer-modeling study. *J Cardiovasc Electrophysiol.* 2018 Feb;29(2):322-327. doi: 10.1111/jce.13363.
44. O'Brien B, Reilly J, Coffey K, González-Suárez A, Quinlan L, van Zyl M. Cardioneuroablation Using Epicardial Pulsed Field Ablation for the Treatment of Atrial Fibrillation. *J. Cardiovasc. Dev. Dis.* 2023, 10(6): 238.
45. Koruth JS, Kuroki K, Iwasawa J, et al. Endocardial ventricular pulsed field ablation: a proof-of-concept preclinical evaluation. *Europace* 2020;22(3):434-439.
46. Verma A, Haines DE, Boersma LV, Sood N, Natale A, Marchlinski FE, Calkins H, Sanders P, Packer DL, Kuck K-H, Hindricks G, Onal B, Cerkevnik J, Tada H, DeLurgio DB, PULSED AF Investigators. Pulsed Field Ablation for the Treatment of Atrial Fibrillation: PULSED AF Pivotal Trial. *Circulation* 2023 May 9;147(19):1422-1432.
47. Driessen, A.; Berger, W.; Krul, S.; van den Berg, N.; Neefs, J.; Piersma, F.; Chan Pin Yin, D.; de Jong, J.; van Boven, WJ.; de Groot, JR. Ganglion Plexus Ablation in Advanced Atrial Fibrillation. The AFACT Study. *J. Am. Coll. Cardiol.* 2016, 68, 1155–1165.
48. Hartl S, Reinsch N, Fütting A, Neven K. Pearls and Pitfalls of Pulsed Field Ablation. *Korean Circ J.* 2023 May;53(5):273-293.
49. Avazzadeh, S.; Dehkordi, M.; Owens, P.; Jalali, A.; O'Brien, B.; Coffey, K.; O'Halloran, M.; Fernhead, H.; Keane, D.; Quinlan, L. Establishing electroporation thresholds for targeted cell specific cardiac ablation in a 2D culture model. *J. Cardiovasc. Electrophysiol.* 2022, 33, 2050–2061.
50. Katritsis, D.G.; Pokushalov, E.; Romanov, A.; Giazitzoglou, E.; Siontis, G.; Po, S.; Camm, J.; Ioannidis, J. Autonomic Denervation Added to Pulmonary Vein Isolation for Paroxysmal Atrial Fibrillation. *J. Am. Coll. Cardiol.* 2013, 62, 2318–2325.
51. Pachon, J.; Pachon, E.; Pachon, J.C.; Lobo, T.; Pachon, M.Z.; Vargas, R.; Jatene, A. “Cardioneuroablation”—new treatment for neurocardiogenic syncope, functional AV block and sinus dysfunction using catheter RF-ablation. *Europace* 2005, 7, 1–13.
52. O'Brien B, Reilly J, Coffey K, González-Suárez A, Buchta P, Buszman PP, Lukasik K, Tri J, van Zyl M, Asirvatham S. Epicardial Pulsed Field Ablation of Ganglionated Plexi: Computational and Pre-Clinical Evaluation of a Bipolar Sub-Xiphoid Catheter for the Treatment of Atrial Fibrillation. *Bioengineering* 2023 Dec 24;11(1):18.